



## Durability assessment of structural sealant glazing systems applying a performance test method

Wilma Wallau & Christoph Recknagel

To cite this article: Wilma Wallau & Christoph Recknagel (2020): Durability assessment of structural sealant glazing systems applying a performance test method, The Journal of Adhesion, DOI: [10.1080/00218464.2020.1840985](https://doi.org/10.1080/00218464.2020.1840985)

To link to this article: <https://doi.org/10.1080/00218464.2020.1840985>



© 2020 Taylor & Francis Group, LLC



Published online: 10 Nov 2020.



Submit your article to this journal [↗](#)



View related articles [↗](#)



View Crossmark data [↗](#)

# Durability assessment of structural sealant glazing systems applying a performance test method

Wilma Wallau  and Christoph Recknagel

Bundesanstalt für Materialforschung und -prüfung, Berlin, Germany

## ABSTRACT

During the service life of a Structural Sealant Glazing (SSG) facade, its silicone bond is simultaneously exposed to climatic and mechanical loads. Current durability assessment methods yet schedule separate test programmes for accelerated weathering and mechanical loading. This study presents a durability test that applies mechanical loading and weather cycling simultaneously simulating 50 years of use. Two common structural sealants are tested. The mechanical behaviour of medium-scale system specimens in tension, compression and shear is recorded for performance assessment during exposure. Moduli and dissipated energies show a characteristic decrease, indicating stress relaxation and degradation. Tensile and shear moduli and strengths of sections cut out from the system specimens after exposure are notably reduced by combined loading compared to those of reference and weathered specimens. Differences between performance and durability characteristics of the two sealants are consistent, also regarding supplementary visual inspection and hardness measurements. The approach introduced in this article provides a basis for more comprehensive performance-related durability testing of SSG-systems.

## ARTICLE HISTORY

Received 5 June 2020  
Accepted 20 October 2020

## KEYWORDS

Structural sealant glazing;  
cyclic weathering;  
mechanical loading; artificial  
ageing; durability  
assessment

## 1. Introduction

Glass facades are a common choice in architectural design of building envelopes of high-rise buildings all over the world. Buildings with a clear representative function often apply structural sealant glazing (SSG), since the adhesive bonding technology avoids frames or clamping elements that would distract a plane appearance of the building envelope. In this way, SSG is a fundamental technical solution for contemporary facade designs. The structural bond between the glass pane of a facade element and the substructure is often applied circumferentially and is commonly formed by a two-component-filled silicone elastomer. The rubber-like bond is designed among others to transmit mechanical loads due to gravity, wind pressure or suction from the facade element to the structure, to damp vibrations, and to withstand mechanical strain due to thermal dilatation. Compared with clamped window

**CONTACT** Wilma Wallau  [wilma.wallau@bam.de](mailto:wilma.wallau@bam.de)  Bundesanstalt für Materialforschung und -prüfung, Berlin 12205, Germany

© 2020 Taylor & Francis Group, LLC

This is an Open Access article distributed under the terms of the Creative Commons Attribution-NonCommercial-NoDerivatives License (<http://creativecommons.org/licenses/by-nc-nd/4.0/>), which permits non-commercial re-use, distribution, and reproduction in any medium, provided the original work is properly cited, and is not altered, transformed, or built upon in any way.

systems or point fixing systems, which transfer heat and cause local accumulation of stresses in the glass pane, SSG-systems reduce heat transfer and stresses in the glass pane. For taking full advantage of the technology, SSG-systems therefore ideally omit retaining devices and mechanical self-weight support of the glass panes. In this case, durability of the structural bond is not only beneficial but rather necessary, as bond failure can be fatal in case of panes dropping from great heights. Indeed, practical experience with SSG-systems indicates sufficiently long service lifetimes.<sup>[1]</sup> However, the durability of structural joints must be approved by building authorities, which raises the question as to how the durability of SSG-systems can be assessed reliably.

### **1.1. Durability testing**

While performance testing of new SSG-systems is feasible and practised, e.g. by exposing mock-ups to design loads as part of the ASTM Standard Guide for SSG,<sup>[2]</sup> durability assessment is considerably more challenging. A comprehensive durability test requires knowledge and technical realisation of all relevant ageing and fatigue provoking loads. The ageing and fatigue mechanisms must be accelerated to obtain test results within a reasonable period of time. However, highly accelerated test protocols can reduce the reliability of the test result. Further, even comprehensive durability testing and factory production control cannot guarantee functioning of every structural bond over the entire presumed service life, since durability is tested on a sample basis. Yet combining durability testing with structural health monitoring approaches, which evaluate the performance of the structural bond during its service life,<sup>[3,4]</sup> may increase the reliability and consequently the acceptance of SSG-systems that abandon mechanical self-weight support and retaining devices.

The current European test and design method ETAG 002<sup>[5]</sup> utilises a defined small-scale specimen, which consists of a glass and metal substrate. The two parts are bonded by the structural silicone joint with a specified geometry. Width (or bite)  $b$  and thickness  $e$  of the bond are 12 mm, the length  $l$  is 50 mm. Tensile and shear strengths of a number of such small-scale specimens are measured to statistically calculate the design stresses of a specific structural silicone sealant which, among others, define the minimum width and thickness of a specific SSG-joint. However, high empirical safety factors like six are applied to compensate for the simplicity of the design approach. To assess, among others, effects of ageing and fatigue, specimens of the same kind are separately subjected to different test protocols. The main artificial ageing test of ETAG 002 involves the immersion for 42 days in water at elevated temperature ( $T = 45\text{ }^{\circ}\text{C}$ ) and simultaneous exposure to UV-radiation through the glass substrate. Additional test protocols address the compatibility of the structural sealant with cleaning products and other

materials used in the SSG-system, like gaskets or weather seals. Fatigue characteristics of the structural bond are tested by applying altogether 5350 tensile stress cycles, that correspond to either 60, 80 or 100 % of the tensile design stress. The tested structural sealant is deemed sufficiently durable when mean tensile and shear strengths of the variously exposed specimens are higher than 75 % of the mean strengths of non-exposed specimens and at least 90 % of the specimens rupture cohesively.<sup>[5]</sup> All these test protocols are conducted separately to assess the effects of specific degradation mechanisms. However, real structures are exposed to multiple loads simultaneously, so that degradation mechanisms interact and possibly amplify one another.<sup>[6]</sup>

Following this approach, a number of durability tests, developed mainly for weather seals, either involve sequential or simultaneous exposure to movement cycles and artificial weathering.<sup>[7–9]</sup> Durability of the tested sealant joint is evaluated from visually examined changes in cohesion, adhesion, and appearance.<sup>[8]</sup> The appearance of a weather seal, though, relates insufficiently to its main performance requirement: tightness.

### **1.2. Performance assessment**

This consideration leads to the concept of performance assessment. Looking for means to “accurately quantify the effects of the environmental degradation factors in laboratory and field tests”,<sup>[10]</sup> researchers developed laboratory and outdoor apparatuses for testing the performance and durability of building joint sealants and understanding ageing and fatigue mechanisms.<sup>[11,12]</sup> One test configuration allows for tensile and compressive strain control of small-scale specimens and in situ monitoring of the transmitted stress.<sup>[10]</sup> An evaluated engineering modulus was regarded as a suitable performance indicator. By systematically varying exposure conditions: ultraviolet radiation (UV), relative humidity, temperature, and strain, the authors then statistically assessed the effects of single and combined degradation factors on the decreasing elastic modulus.<sup>[10]</sup> A similar approach applies natural weathering and cyclic movement simultaneously.<sup>[13]</sup> There, changes of the elastic moduli calculated from the continuously monitored stress-strain behaviour revealed effects of temperature, humidity and damage on the performance of the building joint. All these approaches combine use-related exposure conditions and the measurement of performance-characterising mechanical parameters for studying effects of ageing and/or fatigue.

### **1.3. Structural sealant glazing joint**

SSG-systems mainly are required to maintain their load-bearing capacity throughout their service life. Some works deal with the fatigue behaviour of

structural sealant joints.<sup>[14,15]</sup> Sugiyama studied the fatigue of some sealants with different formulations under tension/compression and shear loads.<sup>[15]</sup> Movement in shear resulted in less mechanical degradation than mechanical cycles in tension/compression mode. Sealants with lower secant moduli had higher fatigue life, which the author attributes to the displacement-controlled fatigue loading.<sup>[15]</sup> Omitting fatigue effects, another study focussed on artificial accelerated ageing, with weathering cycles between high temperature and humidity ( $T = 85\text{ }^{\circ}\text{C}$ , r.h. = 85 %) and low temperature ( $T = -40\text{ }^{\circ}\text{C}$ ) and humidity intervals.<sup>[16]</sup> While pure exposure to high temperature and humidity led to decreased tensile bond strength, weather cycling did not notably affect the tensile strength of specimens after different test durations, which the authors attribute to shorter absolute exposure times at elevated temperature during a weather cycle, compared to pure storage at high temperature. Indeed, this test omits mechanical loads, yet the structural sealant bond must bear mechanical loads during exposure, damp vibrations and always prevent direct contact of the adherents. Hence, multiple mechanical characteristics and parameters are relevant for performance assessment of SSG-systems, such as stiffness, elasticity and damping, creep, relaxation and strength characteristics. A recent study focussed on the dynamic compressive creep behaviour of an aluminium-to-aluminium structural silicone bond.<sup>[17]</sup> The authors evaluated the maximum stress transmitted and the energy absorbed by the bond for the applied dynamic compressive load cycles to strains of 60–80 %. Referred to their initial value, both parameters decrease similarly with the number of load cycles. However, the energy absorbed by the bond decreases more strongly.<sup>[17]</sup>

#### **1.4. New performance and durability test method**

Little is known about the effects of combined exposure to weathering and mechanical cycling on the performance and durability of SSG-systems. This contribution addresses this research gap by suggesting a new performance and durability test and applying it to a common SSG-system using two different structural sealants.

Although it is challenging, if possible at all, to suggest loading parameters which represent a wide range of possible exposure conditions, it was attempted to design such a generalised durability test.<sup>[18,19]</sup> Supposing a model case building (Figure 1a), different design features and load scenarios were considered and combined following a worst-case approach to develop a test procedure that realises simultaneous weathering and mechanical loading (Figure 1b). Specifically designed medium-scale specimens (Figure 2), referred to as *system specimens*, resemble a segment of a common SSG-bond. Length  $l = 400\text{ mm}$  and thickness  $e = 6\text{ mm}$  of the silicone bond deviate from that of ETAG-specimens, while the width

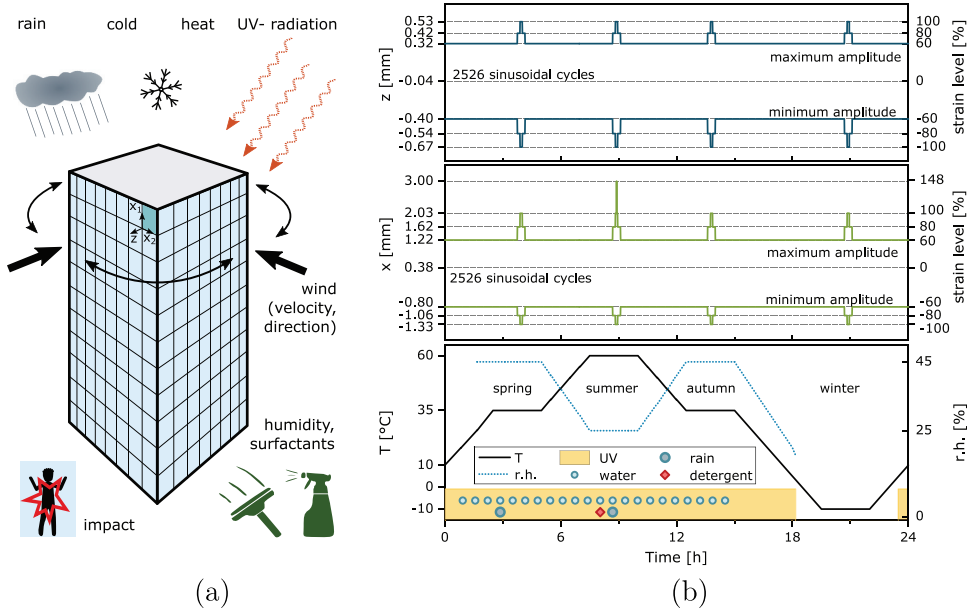


**Figure 1.** Loads applying to the SSG-facade of a model case building (a), which were considered in the combined mechanical and climatic load function simulating a year of real exposure (b).

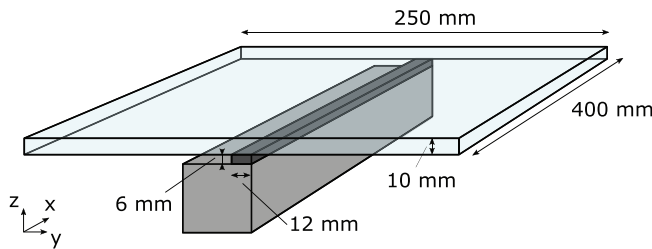


**Figure 2.** System specimen: sealant bead between glass pane and aluminium frame (40x40x400 mm<sup>3</sup>).

$b = 12$  mm is the same. Two-dimensional mechanical loading of the system specimens in  $x$ - and  $z$ -direction provoke a system response in the form of the resulting forces, which are measured for performance assessment during exposure. Details on the development of the test are given in a previous publication.<sup>[19]</sup>

One of the main goals of this study is the interpretation of the system response during laboratory exposure. The paper further studies effects of combined mechanical and climatic exposure on the conventional mechanical characteristics from tensile and shear tests in comparison with those of non-exposed reference specimens and specimens exposed only to the climatic loading function. Supplementary results from visual inspection of the joint and hardness measurements are presented for complementing the interpretation of the test results.

## 2. Experimental procedure

Two test series (A and B) were conducted in this study, applying either a stiffer structural sealant *a* or a less stiff structural sealant *b*. Both sealants are commercial products for application in SSG-systems. Table 1 lists some specifying properties which were measured for the cured sealants.

The system specimens were manufactured from an anodised aluminium square bar, a float glass pane, and the two-component structural silicone sealant following instructions of the sealant supplier.<sup>[20]</sup> After application of primer on the cleaned surfaces of the adherends, a masked spacer and clamps were arranged to define the volume of the joint. Masking tape was applied on surfaces adjacent to the joint, before the volume was filled with the two-component silicone using a Sulzer Mixpac DXH dispenser. Excess sealant and masking tape were then removed immediately and the specimens cured at ambient conditions ( $T = 15...19\text{ }^{\circ}\text{C}$  and  $r.h. = 45...60\%$ ) for at least 6 hours. After curing, the system specimens remained stored indoors for about a year while all necessary preparations for the durability test were made. Each test series involved the simultaneous exposure of two specimens to combined loading, meaning simultaneous mechanical loading and weathering. Combined loading was realised with a mechanical loading device (Figure 3) with two actuators, which was arranged inside a climate cabinet. An extra specimen was placed in a weathering rack in the same climate cabinet next to the mechanical loading device, so that it would be subjected to weathering only. A fourth specimen remained non-exposed for reference.

Superimposed weathering and mechanical loading, as shown in Figure 1b, comprised at least 50 climatic cycles, e.g. 50 real days of combined exposure. When technical problems requiring an interruption of loading occurred during the test, the overall test duration was prolonged by an extra climatic cycle. Subsequently, a set of impact events was simulated at ambient temperatures between 21 and 27 °C by sinusoidal cycles in x- and z-direction; with  $x = -1.86...0.95\text{ mm}$  and  $z = -1.05...1.33\text{ mm}$ . In series A, eight load cycles were applied at increasing frequencies of 5, 10, 20, and 30 Hz. As the mechanical loading device satisfied the required dynamic characteristics well at  $f = 10$  and 20 Hz, impact events in series B only comprised two cycles at 10 Hz and one at 20 Hz. Following the impact events, additional combined load cycles were applied.

**Table 1.** Technical specifications of the sealants.

standard	property	sealant <i>a</i>	sealant <i>b</i>
ISO 868	Shore A	45.0	38.3
ISO 1183-1 (A)	Density [ $\text{g}/\text{cm}^3$ ]	1.31	1.37
ISO 527	Tensile strength [ $\text{N}/\text{mm}^2$ ]	2.11	1.58
ISO 527	Yield strain [%]	236	192
ISO 527	Elastic modulus [ $\text{N}/\text{mm}^2$ ]	4.12	3.35



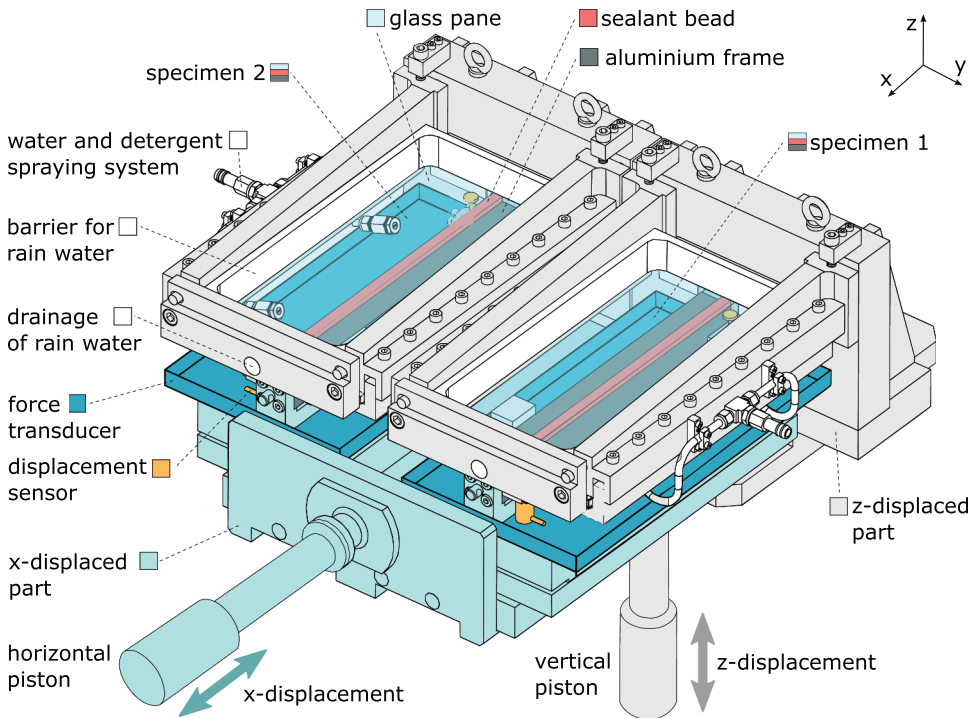


**Figure 3.** Mechanical loading device with two system specimens; arranged in a climate cabinet for combined mechanical and climatic exposure.

### 2.1. Climatic loading function

A climatic cycle involved the simultaneous variation of several climatic operating conditions, as depicted in Figure 1b. The glass panes of the specimens were exposed to 22 rain events lasting 1 min and to UV-radiation from UV-A-lamps which were arranged at the ceiling of the climate cabinet. Radiant emittance of the installed fluorescent UV-A lamps depends on their service lifetime and more strongly on operating temperature. The irradiance measured close to the glass pane decreased to about 80–90 % of its initial value of about  $8 \text{ W/m}^2$ , and by  $-1 \text{ \%}/\text{K}$  at  $T > 20 \text{ }^\circ\text{C}$ . Furthermore, deionised water and/or detergent were sprayed onto one side of the sealant bead of each specimen. The same side of the sealant bead was exposed to extra UV-radiation from compact UV-lamps (320–400 nm), which were arranged at the three open sides.

During 'winter', UV-lamps did not operate; humidity, water, and detergent were not fed in to avoid formation of ice. Occasionally, water which was not withdrawn from the system in time froze in proximity of the structural bond, the displacement sensors, and the load cells. In these cases, the test was interrupted for removal of ice and dehumidification was generally intensified before cold periods.



## 2.2. Mechanical loading function

In the mechanical loading device, shown in [Figure 3](#), the glass panes of the system specimens were clamped to the crosshead, which was displaced in z-direction by the vertical hydraulic actuator. The aluminium profiles of the specimens were mounted to a two-dimensional load cell each, which measured the transmitted forces in x- and z-direction. The load cells were again attached to the bottom plate of a sliding carriage, which was displaced in x-direction by a horizontal hydraulic actuator. Two LVDT sensors, positioned at the weathered side of the 400 mm sealant bead at  $x = 20$  mm and  $x = 380$  mm, measured the z-displacement of the sealant joint. A third displacement sensor was positioned horizontally at  $x = 330$  mm for measuring the x-displacement between the glass pane and the aluminium frame. A multi-channel unit controlled x- and z-displacement of the sealant joint of specimen 1, with the sensor located closer to the vertical piston giving the actual z-value. The mechanical loading device with the two hydraulic actuators, bearings and sliding carriages operated highly satisfactorily allowing precise control of the set displacement cycles.

At elevated temperatures, actual displacements deviated by up to  $-4$  to  $+2.5$  % (z-direction) and  $-1.5$  to  $+0.2$  % (x-direction) from the set value. Caused by the compliance of the z-displaced part and clearance of the ball bearing, both specimens were deformed less on the side located further from the vertical piston: by up to 30 (compression) and 75 % (tension) of the set value. Further, average tensile and compression loading of specimen 1 was slightly less severe than that of specimen 2 (up to  $-10$  and  $+20$  %). Amplitudes of x-displacement of specimen 2 deviated by only  $-4$  to  $+4$  % from those of specimen 1. Additionally, the strain and force measurements include a small linearity error and a temperature error, which could not be compensated by the measurement and control system. The actual displacement thus varied from the measured displacement affecting the real mechanical loading function. At the same time, changing ambient conditions lead to volume changes of the sealant bead, also affecting the actual stress state in the bond.<sup>[19]</sup>

However, evaluation of the system response should give qualitative information on relative changes of characteristic mechanical parameters over the course of the test. Irrespective of exact measurement uncertainties, when only considering mechanical cycles that occur at the same temperature level, it is possible to exclude a temperature-induced error of stress and strain. Thus, relative changes of characteristic parameters were assessed that further were refined by only considering mechanical cycles that apply the same strain level.

## 2.3. Continuous characterisation

The displacement and force signals in x- and z-direction form a set of consecutive hysteresis curves or mechanical cycles. A mechanical cycle here is

defined as a sine cycle of the displacement signal. The z-displacement of a system specimen is calculated from the mean of the two measured values. Each mechanical cycle has characteristic dynamic mechanical parameters, as illustrated in Figure 4. In the applied range of deformations, the system response is approximatively linear allowing calculation of an elastic modulus

$$M = \frac{\Delta F}{\Delta s} \frac{e}{A_0} \quad (1)$$

from engineering stress  $\Delta F/A_0$  and strain  $\Delta s/e$ , with the thickness of the structural bond  $e$  and the bond area  $A_0$ . The dynamic modulus  $M_{dyn}$ , calculated from the maximum and minimum forces  $F$  and displacements  $s$  measured during a mechanical cycle, describes the tensile and compression modulus  $E_{dyn}$  in z-direction and the shear modulus  $G_{dyn}$  in x-direction. To identify the performance in tension, compression, and shear more specifically, the moduli were calculated only from the according positive ( $F > 0$ ) or negative ( $F < 0$ ) part of the hysteresis loop. The maximum or minimum forces and displacements were then referred to  $F = 0$  and the mean displacement at zero force  $\bar{s}_{F=0}$ , yielding the tensile modulus  $E_t$  and compression modulus  $E_c$  in z-direction, and the positive and negative shear moduli  $G_{pos}$  and  $G_{neg}$  in x-direction. Every mechanical cycle was further characterised by its dissipated energy

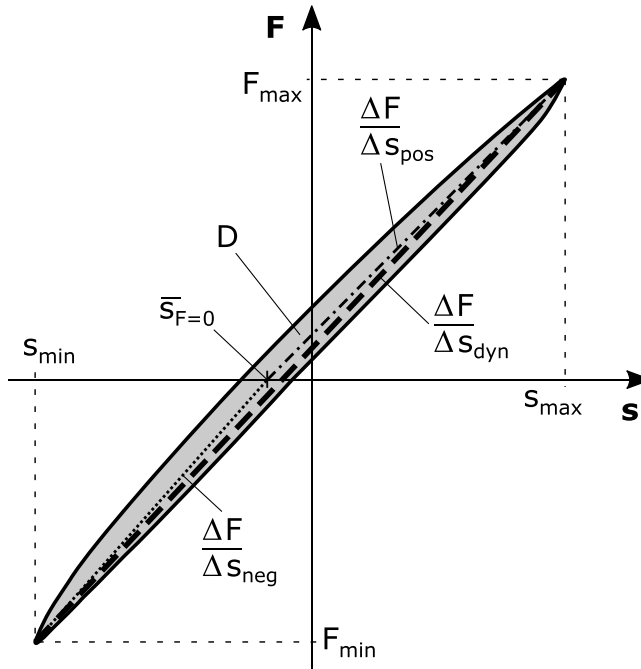


**Figure 4.** Calculation of characteristic mechanical parameters from the force-displacement data of a mechanical cycle for  $s = x, z$  and  $F = F_x, F_z$ .

$$D = \int F ds, \quad (2)$$

which corresponds to the integral area of its hysteresis loop. This lost energy relates to the damping capacity of the system. For obtaining a high temporal resolution of the measurement data, 410 values were recorded per mechanical cycle. The considerable data volume of a complete durability test was evaluated with Octave scripts.

#### 2.4. Discontinuous characterisation

Discontinuous characterisation refers to visual inspection and hardness measurements during exposure. Regularly, every few climatic cycles when the set temperature has reached 20 °C and set displacements were zero, the testing procedure was paused for inspection intervals. During the inspection intervals, which lasted 20 min at most, the integrity of the specimens was examined. Further, shore A hardness was measured on the accessible and weathered side of the sealant bead midway between the adherents at  $x = 70, 200$  and  $330$  mm, at indentation times of 3 s, and sealant temperatures between 17 and 23 °C. The handheld durometer was applied horizontally by the same experienced worker to minimise uncertainties. After resetting the piston to its initial position at the start of the durability test and successively zeroing all displacement sensors, combined loading was continued. Potential flaws or cracks on the accessible side on the structural bond were detected with an endoscope while the bond was being deformed.

Discontinuous characterisation further also refers to conventional hardness measurements, visual inspection of the system specimens, and shear and tensile tests, which were conducted after the durability test. The system specimens were bent up slightly to make potential cracks and notches visible for photographic documentation. All system specimens were then water jet cut into small-scale specimens according to the regular cutting scheme illustrated in [Figure 5](#). System specimen 2 of series A, whose glass pane broke during the durability test, was cut according to the customised scheme. The 50 mm-long sections were subjected to tensile and shear tests at  $T = 20$  °C and strain rate = 5 mm/min. From the stress–strain curves of the tensile and shear tests characteristic mechanical parameters were evaluated: the strength (maximum stress) and the associated yield strain as well as the moduli (mean derivative of the stress-strain results at strains below 0.02). Additional Shore A hardness measurements of the structural sealant from all system specimens were conducted after the durability test on two samples per 75 mm-section, shown in [Figure 5](#). The indentation time of nine repeated measurements per sample was 3 s.

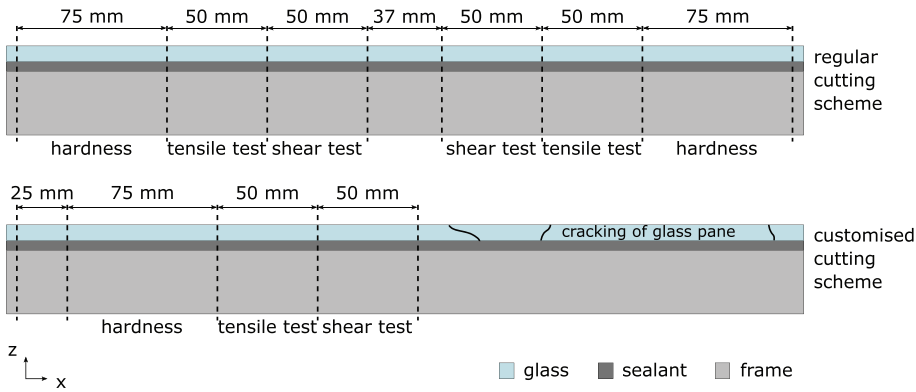


**Figure 5.** Cutting scheme of the system specimens for obtaining small-scale specimens for mechanical characterisation.

### 3. Results and discussion

This section aims to assess and compare performance and durability characteristics of two structural sealants, based on the experimental results of series A and B. These include the continuous mechanical characterisation during combined mechanical and climatic loading of two system specimens per series. Further, results of discontinuous characterisation of differently exposed specimens and sealant material are presented and discussed.

Applying the approach of ETAG 002, durability assessment of the two structural sealants is based on results of tensile and shear tests. Statistical significance of the results presented in this study is limited, as mean values are calculated from the strengths of only two to four small-scale specimens, while ETAG 002 schedules a number of 10 specimens for assessing effects of artificial ageing and mechanical fatigue. Accordingly, the test series only yield indications on the durability characteristics of the two sealants and no conclusive result.

#### 3.1. Continuous mechanical characterisation

First assessment of the continuously monitored system response reveals that maximum and minimum forces in x- and z-direction oscillate with the ambient conditions during a climatic cycle. In addition, the absolute values of the measured forces expectedly increase with the strain level. Another paper, which deals with performance assessment of SSG-joints, discusses these aspects in more detail.<sup>[19]</sup> This paper focusses on how the performance of the system specimens changes throughout the durability test. The following section discusses effects on the moduli.

##### 3.1.1. Moduli

To circumvent influences of ambient conditions and strain level on the system response, only intervals at constant amplitude level (100 %) and set

temperature (35 °C) are considered in Figure 6, which shows the dynamic moduli over the climatic cycles. In both series, the moduli  $E_{\text{Dyn}}$ , corresponding to the overall vertical deformation in z-direction, are higher than the shear moduli  $G_{\text{dyn}}$  by factors between 6 and 8. Both the dimension of the system specimens and the constitutive difference between shear and tensile elastic material properties contribute to this difference.<sup>[21]</sup> As expected, all moduli of series A specimens are higher than those of the specimens manufactured with the less stiff sealant tested in series B. The ETAG fatigue test applies force-controlled loads, as usual in fatigue testing. Here, a displacement-controlled load function is chosen, which is advantageous regarding the technical implementation of repeatable and safe simultaneous servo-hydraulic mechanical loading of two system specimens. Both series were exposed to the same load function. As this load function was derived for the stiffer sealant applied in series A, one could argue that the specimens of series B were thus exposed to relatively lower loads, which again influences the system response. This aspect will be revisited in section 3.2.

The dynamic moduli decrease most during the first climatic cycles. Dynamic stress relaxation of the filled silicone elastomers mainly causes this settling behaviour. A previous study showed that stress relaxation and modulus recovery occur at all three different strain amplitudes.<sup>[19]</sup> In this way, previous loading influences the system response. As ambient conditions also

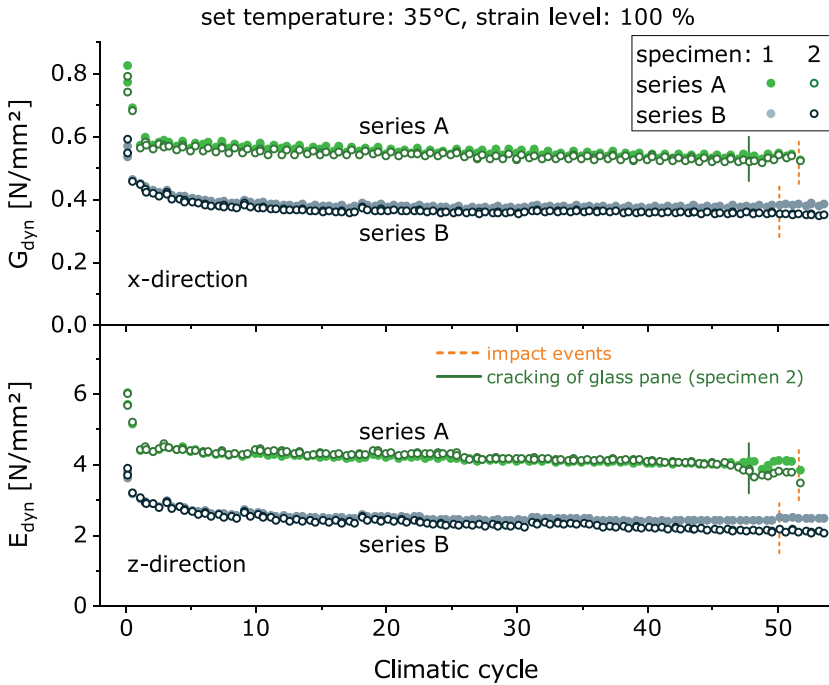


**Figure 6.** Dynamic moduli of series A and B specimens in x- and z-direction at set temperature  $T = 35\text{ °C}$  and strain level = 100 % over test duration; every 10th mechanical cycle.

affect the dynamic mechanical characteristics and volume of the sealant, various effective load combinations occur during a 24 h climatic cycle. Hence, the specimens have only been exposed to all possible load combinations after the first climatic cycle. As Figure 6 indicates, stress relaxation of the stiffer specimens of series A occurs within about one climatic cycle, whereas the initial moduli decrease in series B takes about 10 climatic cycles. After settling, the moduli of all specimens continue to decrease, yet at a low rate. There, moduli of the series A specimens decrease at a slightly higher rate compared to that of series B.

Occasionally, the dynamic moduli shift slightly. These unintended positive or negative offsets between loading intervals result from the reset of the piston position and zeroing of the displacement sensors after an inspection interval at slightly different temperatures.

In series A, the dynamic modulus in z-direction  $E_{\text{dyn}}$  of specimen 2 drops during the winter period of the 48th climatic cycle. At this time, the z-force signal of the machine exceeded its limit value and loading was paused automatically, which possibly coincides with the formation of cracks in the glass pane of specimen 2 which were noticed later. During the cold periods of previous climatic cycles, the force signal already showed an anomalous course. Formation of ice on the exposed sealant and the glass pane due to leakage of water at freezing temperatures is a possible cause of the cracking. Despite the cracks across the whole width of the circumferentially clamped glass pane, loading could be continued. The system response in x-direction is not even notably affected. The moduli of the two system specimens of series A closely resemble each other. Dynamic moduli of the series B specimens deviate slightly towards longer exposure times, both in x- and z-direction.

The dynamic moduli in tension ( $E_t$ ) and compression ( $E_c$ ), and the dynamic shear moduli in positive ( $G_{\text{pos}}$ ) and negative ( $G_{\text{neg}}$ ) load direction of specimen 1 are depicted in Figure 7. In both series, the two shear moduli in positive and negative load direction resemble, while the compression moduli are notably higher than the tension moduli. The shear loads in positive and negative direction practically mean the same load scenario. They only differ slightly regarding the absolute displacement amplitude, as shown in Figure 1. Compression and tension, on the other hand, are fundamentally different types of loading. Under compression, filled silicone elastomers generally behave stiffer than under tension and shear.<sup>[22,23]</sup> Although a clear interpretation of the tensile and compression moduli is hindered due to the offsets after inspection intervals, it appears that compression and tensile moduli converge towards the end of the test duration. This is confirmed by results from sectional evaluation of the slope of the tensile and compression moduli during the testing time between inspections. Such evaluations show that throughout the test duration, compression moduli decrease more strongly than tensile

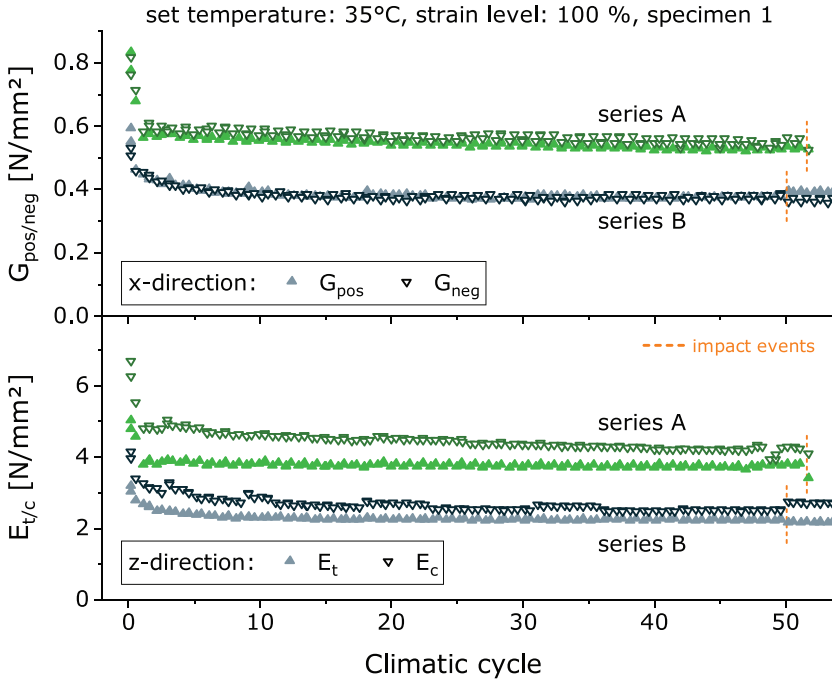


**Figure 7.** Tension, compression and shear moduli of series A and B specimen 1 at set temperature  $T = 35^\circ\text{C}$  and strain level = 100 % over test duration; every 10th mechanical cycle.

moduli in both series. The sectional evaluation further reveals that the tensile and the compression modulus of series B decrease at a higher rate than the respective modulus of series A. These differences between the system response of the two series can be ascribed to different stress relaxation characteristics of the two structural sealants. They might also reflect a possibly increased susceptibility of sealant *b* to ageing and fatigue.

Throughout the test duration, the courses of all moduli indicate that the specimens of series A and B withstand the combined loading including the impact loads at the end of the test without spontaneous failure. All moduli associated with series A are generally higher than those of series B specimens, which reveals the superior load-bearing capacity of sealant *a*. However, the absence of a characteristic accelerating decline of the moduli, which is typical in fatigue testing, implies that the specimens bear the combined loads imposed during testing. Despite small shifts after the impact events and the cracking of the glass pane of specimen 2, the moduli continue the previous steady course. All specimens of series A and B withstand at least 131.2 and 136.5 thousand mechanical cycles at simultaneous weather cycling. During combined exposure, all moduli decrease significantly compared to their initial values. After an initial phase of stress relaxation, the moduli can be assumed to reflect the performance of a common SSG-joint during its service life.



### 3.1.2. Dissipated energies

Another dynamic mechanical parameter, the dissipated energy, relates to the ability of the joint to absorb and damp mechanical energy. Figure 8 shows the dissipated energies of the climatic cycles which correspond to intervals when the set temperature is 35 °C and the strain level is 100 %. As can be seen from Figure 8, more energy dissipates during load cycles in x- than in z-direction, which is related to the higher amplitudes of x-displacement. During combined exposure, specimens from the stiffer sealant tested in series A generally exhibit higher dissipated energies than those of series B. Sealant *a*, thus, has a higher damping capacity than sealant *b*, throughout the entire test duration. The general course of the dissipated energies over testing time is similar to the decelerating decline of the dynamic moduli (Figure 6). Again, dissipated energies decrease more strongly during the initial stress softening behaviour.

Some signals are disturbed due to the offsets which are associated with the inspection intervals. These offsets make it difficult to interpret the course in detail. However, it becomes apparent from the less affected results of the system response in z-direction of specimen 1, that the dissipated energies continue to decrease throughout the test duration. Figure 9 shows these selected results for cycles at the three strain levels for the set temperature 35 °C (top part) and of cycles at 60 % strain level for the three temperature levels. The energies increase quasi proportionally with the strain level, which is to be

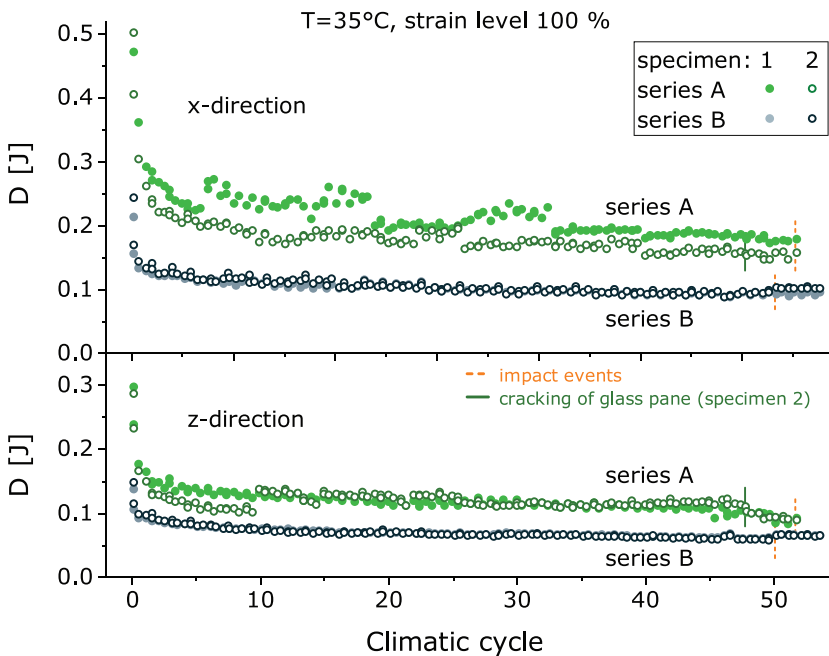


**Figure 8.** Dissipated energies of of series A and B specimens in x- and z-direction at set temperature  $T = 35^{\circ}\text{C}$  and strain level = 100 % over test duration; every 10th mechanical cycle.

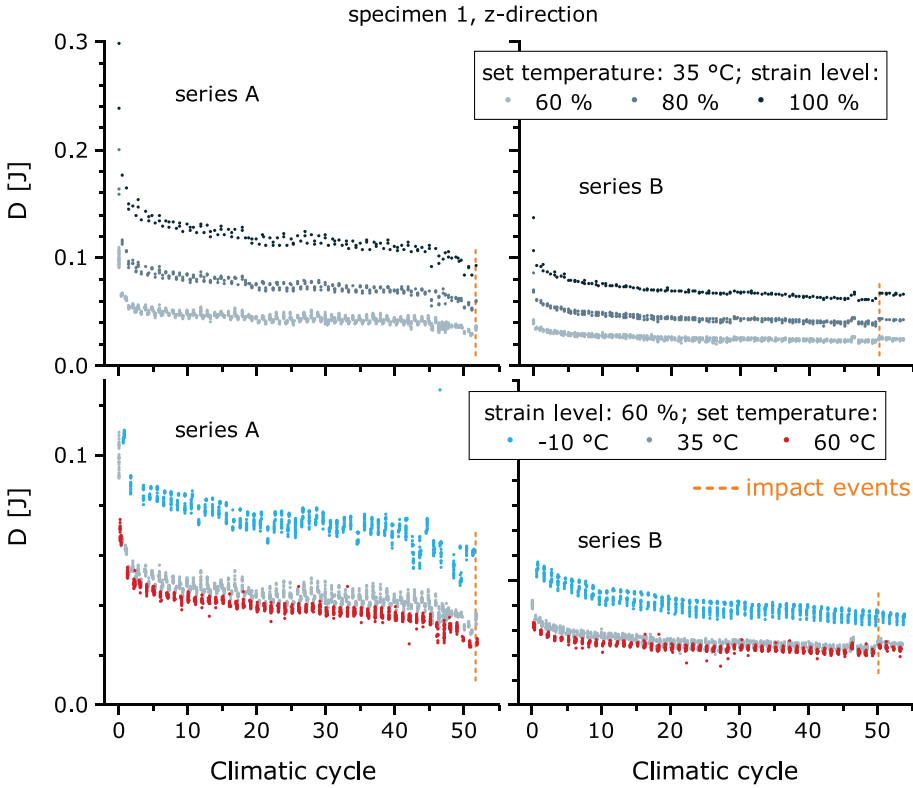


**Figure 9.** Dissipated energies of mechanical cycles in z-direction of specimen 1 of series A and B at constant  $T = 35\text{ °C}$  and varying strain level (top) and constant strain level = 60 % and varying temperature (bottom); every 10th mechanical cycle.

expected as the absolute energy input also increases with the strain amplitude. The initial decrease takes longer for the high amplitude cycles. This again can be ascribed to the fact that high amplitude mechanical cycles occur less frequently than mechanical cycles with lower amplitudes (Figure 1). Figure 9 further shows that the dissipated energy decreases with increasing temperature, particularly regarding the temperature step between  $-10$  and  $35\text{ °C}$ , supporting previous research.<sup>[24]</sup> Towards the end of the test duration, dissipated energies in z-direction of series A specimens (Figure 8) decrease again, while those of the series B specimens continue the previous slightly decreasing trend. The course of these dissipated energies of specimen 1 of series A given in Figure 9 resembles the common behaviour of mechanical parameters during strain-controlled fatigue tests, with a decelerating decline in the beginning, a linear decrease during a second phase, and an accelerating decline towards the end of the test. The dissipated energy decreases at all temperature and strain levels. Malfunctioning of the climate control like formation of ice possibly affecting the specimen or force transducer cannot explain this behaviour. Also, cracking of the simultaneously loaded specimen 2 does not affect the displacement-controlled loading of specimen 1. The results must be

interpreted cautiously due to possible offsets of the signals caused by resets after inspection. However, the course of the dissipated energy indicates a decreasing damping capacity of specimen 1 in series A, which could be related to degradation of the structural sealant due to cyclic weathering and mechanical loading. Note that even at the end of the test, dissipated energies of series A specimens are still higher than those of series B specimens.

While dynamic moduli are calculated from peak strain and stress values only, calculation of dissipated energies incorporates all stress-strain data of a mechanical cycle. It is perceivable that the dissipated energies are therefore particularly susceptible to changes in the mechanical response of the system specimen. Hence, they can be a useful dynamic mechanical parameter for continuous characterisation and early notice of ageing and fatigue effects in durability testing.

### 3.2. Discontinuous characterisation

#### 3.2.1. Tensile and shear tests

From tensile and shear tests of small-scale specimens, which were cut from the system specimens according to the cutting scheme shown in Figure 5, characteristic parameters were obtained. The tensile and shear strength, modulus and yield strain are given in Figures 10 and 11. In accordance with the dynamic moduli recorded during testing, small-scale specimens of series A show higher moduli than those of series B. They also exhibit higher shear and tensile strength and yield strain in all cases of exposure. While tensile strengths of reference specimens and those which were subjected only to climatic loading do not differ significantly, combined loading leads to a notable reduction of the tensile strength of specimens both from series

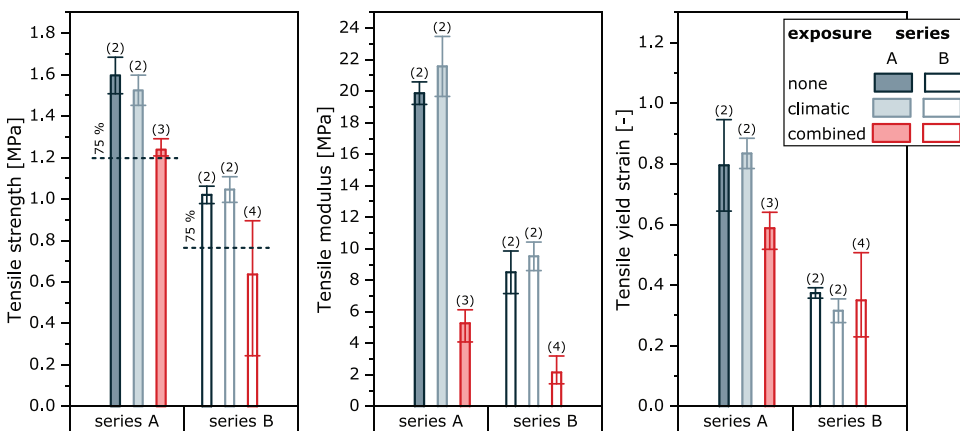


**Figure 10.** Characteristic parameters of tensile tests of small-scale specimens (number of specimens given in brackets) from series A and B; dashed line marks 75 % of the mean tensile strength of the non-exposed reference.

A and B. Shear strengths show comparable results. Deviations of tensile and shear strengths between the three or four sections from specimens which were subjected to combined loading are mostly high. It should be noted that deviations between mechanical characteristics of such samples are generally high, which is usually compensated by testing a larger number of samples.

The configuration of the mechanical testing device could contribute to high deviations of the parameters at combined loading. Sections from the system specimen, which were positioned closer to the vertical piston during exposure, where vertical deformation is higher, mostly have lower tensile and shear strengths. It is perceivable that intensified loading of the bond results in reduced strengths. In series B, it further stands out that sections from system specimen 2 exhibit systematically lower tensile and shear strengths than those of specimen 1. This discrepancy could either be attributed to the effectively slightly more severe tensile and compressive loading of specimen 2 or to possibly weaker bond characteristics of system specimen 2. As the maximum shear strength, which is associated with a section from specimen 1, even lies above the maximum strength of the reference, it appears that not only previous exposure but also specific conditions during manufacturing, curing, or storage influence the mechanical characteristics.

With the smaller bond thickness of the small-scale specimens compared to that of ETAG-specimens, the stress-strain behaviour also differs. Nevertheless, the 75 % durability criterion for tensile and shear strengths of ETAG 002 is applied here. As can be seen from Figure 11, mean shear strengths of all series and exposures exceed 75 % of the mean strength of the reference specimens. Mean tensile strengths (Figure 10) of series A specimens exposed to combined loading are also above the limit, whereas series B specimens after combined exposure show values below 75 %. These different results of shear and tensile tests in series B indicate that tensile characteristics are more susceptible to degradation of SSG-bonds than shear characteristics.

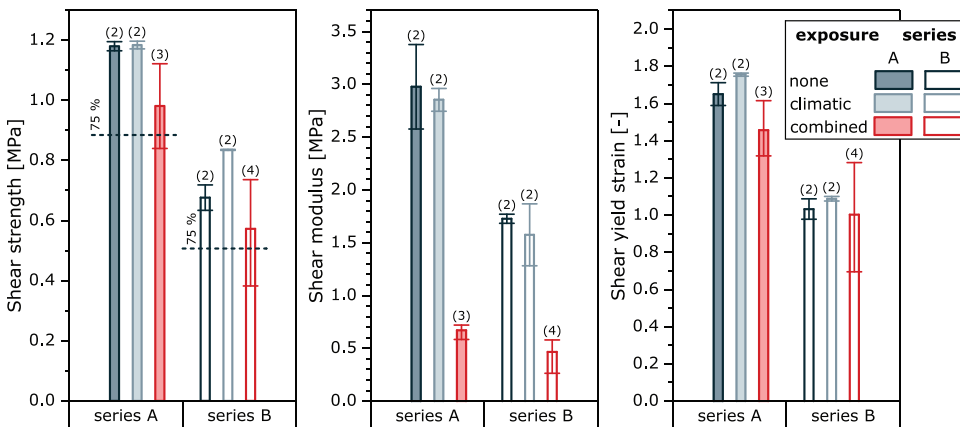


**Figure 11.** Characteristic parameters of shear tests of small-scale specimens (number of specimens given in brackets) from series A and B; dashed line marks 75 % of the mean shear strength of the non-exposed reference.

The other ETAG durability criterion concerns the type of failure: the crack of at least 90 % of the specimens must be located in the sealant, which identifies cohesive failure. [Figure 12](#) shows the ruptured sealant surface of selected small-scale specimens after tensile and shear testing. The crack surface of series B sealant shows a slightly porous texture and the presence of small white particles for all types of exposure. Instead, the crack surfaces in series A are rather smooth showing fine white streaks presumably stemming from mixing of the two components. The small-scale specimens exposed to combined loading ruptured cohesively in series A and mostly adhesively in series B, both in tensile and shear testing. It should be noted that a small-scale specimen from series B exposed only to climatic loading also ruptured adhesively during tensile testing, as shown in [Figure 12](#). Accordingly, the sealant tested in series B must be assessed insufficiently durable, particularly when considering the small number of tested specimens.

Another possible explanation for differences between the two series concerns the test design. The series only differ regarding the type of sealant. Dimensions of the bond and load functions are the same. As indicated above, by applying the same strain amplitude in series B as in series A, in which tensile and shear moduli are higher, the absolute stress transmitted to series B specimens is lower. At the same time, strengths of the ETAG-like small-scale specimens are significantly higher in series A than in series B. According to ETAG 002, the design stress, which determines the loads applied during fatigue testing, is calculated from the strength of non-exposed ETAG-specimens, applying safety factors such as six. This same principle is

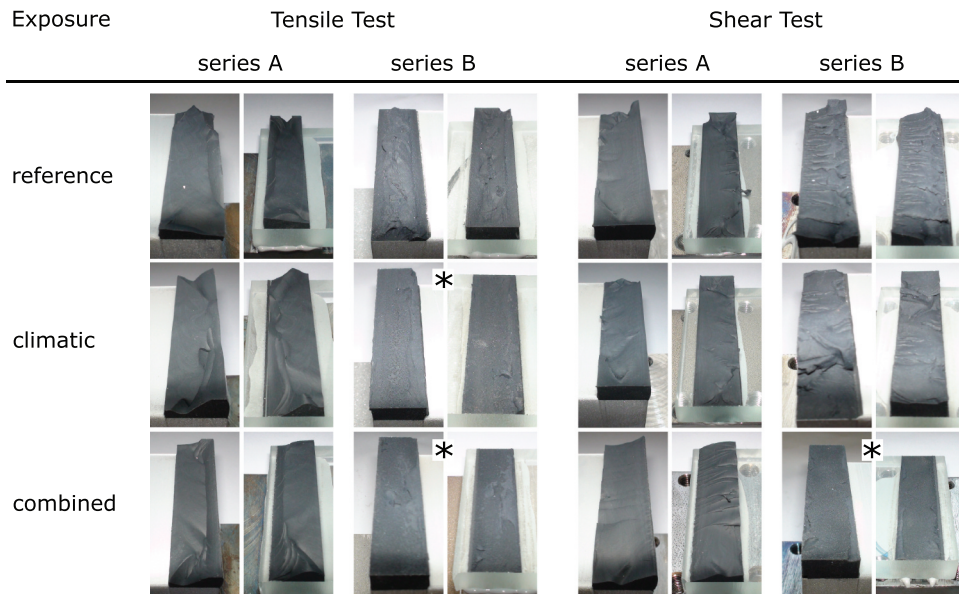


**Figure 12.** Ruptured sealant surface on the metal and glass substrate of small-scale specimens after shear and tensile tests; asterisk denotes adhesive failure.

adopted in the following to estimate which series was subjected to effectively more severe loading. The applied stress  $\sigma$  and the strength  $\sigma^*$  of series A and B can be compared:

$$\frac{\sigma_A}{\sigma_A^*} = f \frac{\sigma_B}{\sigma_B^*}, \quad (3)$$

by evaluating the factor  $f$ . Presuming that both series applied the same strain  $\varepsilon$  during combined loading and assuming linear elasticity  $\sigma = M \cdot \varepsilon$ , equation (3) can be solved for  $f$  by plugging in the mean strengths and respective mean moduli, e.g. of the non-exposed samples depicted in [Figures 10 and 11](#). According to this simple estimation, specimens of series A are subjected to relatively higher tensile loads than series B. An analogous comparison of shear strength and moduli of the sections from system specimens shows that the relative shear loading of series A and B is similar. Although specimens of series B are exposed to less severe tensile loading than those of series A, the mean tensile strengths in series B exposed to combined loading are notably lower, which confirms an increased susceptibility of sealant  $b$  to combined loading.

Comparing mechanical parameters of weathered and reference samples, minor differences become apparent. Weathered samples in some cases have higher strengths, and strains at break compared to the reference samples. The mean values are similar, particularly with respect to common deviation between the mechanical parameters of SSG-specimens. Even a complex weathering cycle combining multiple weathering factors, like the one applied here, does not affect characteristic mechanical parameters as much as the simultaneous mechanical and climatic cycling. This raises the question of whether a solitary accelerated ageing test as scheduled in ETAG 002 realises sufficient loading.

### 3.2.2. Hardness

Results from conventional hardness measurements of the silicone elastomer cut from exposed and reference system specimens are shown in the left part of [Figure 13](#). In series A, weather cycling alone does not cause notable changes of hardness compared to the reference, suggesting high weatherability of the tested sealant. Weathered series B material is even harder than the reference material. It must be noted that hardness of sealant material from the two system specimens of series B that were exposed to combined loading differs too, indicating differences between the individual specimens.

The right part of [Figure 13](#) depicts the results of hardness measurements conducted on the sealant surface of the specimens during inspection intervals. There, significant deviations between the measurement events stand out, which could be related to the manual application of the durometer. In both series, the sealant bead which was only exposed to climatic loading shows higher hardness results than the silicone joint subjected to combined loading for most of the measurement events. Hardness of the stiffer sealant of series

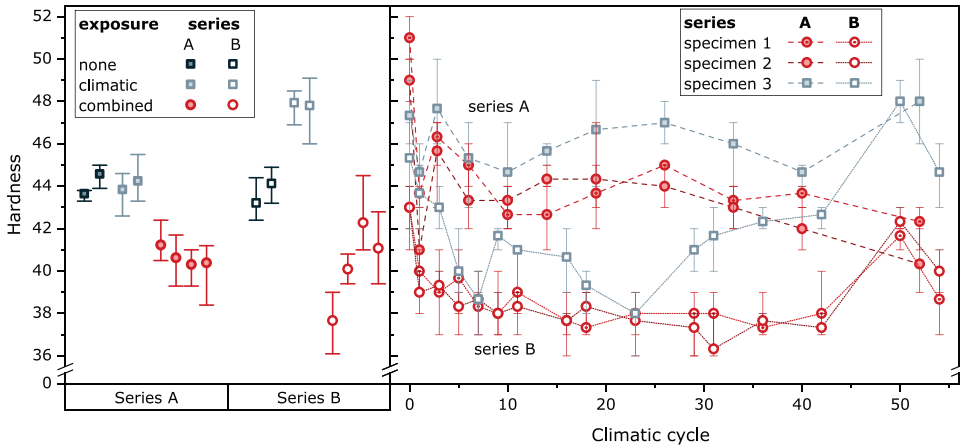


**Figure 13.** Hardness of exposed and non-exposed sealant material (left) and hardness of the sealant surface of the exposed system specimens measured during inspection intervals (right).

A expectedly is higher than that of series B. These results consist with the decreasing dynamic moduli during combined exposure and the reduced elastic moduli from tensile and shear tests.

### 3.2.3. Visual inspection

During the first mechanical cycles after an inspection interval, the accessible side of the sealant bead of the system specimens was examined. With increasing test durations, all specimens exposed to combined loading show notches and cracks at both end sections, meaning the surface of 2 cm from both ends and the two  $12 \times 6 \text{ mm}^2$ -front faces. There, cracks form mostly close to the bond area, where local stress is highest. In some cases, these cracks and notches widen and deepen during of the test.

Examination of the silicone beads after exposure, showed that the centre part is mostly less affected than the end sections. The specimens of series A show no cracks in this centre part whereas the specimens of series B that were exposed to combined loading exhibit cracks on the surface. Figure 14 shows the cracks on the sealant beads of all series B specimens. The bond area at the aluminium adherend of specimen 2 is particularly damaged on the side close to the vertical piston where absolute displacement is higher. There, cracks are several millimetres deep. The crack at  $x \approx 40 \text{ mm}$  even spans across the entire initial bond area.

Considering that mechanical loading in series B is relatively less severe than in series A, stronger crack formation in series B is probably related to weaker bond characteristics of the specimens. With small-scale specimens exposed to combined loading rupturing cohesively in series A and adhesively in series B, the type of failure correlates with the results from visual inspection. The strong deviations in shear and tensile strength in series B (Figures 10 and 11) can be



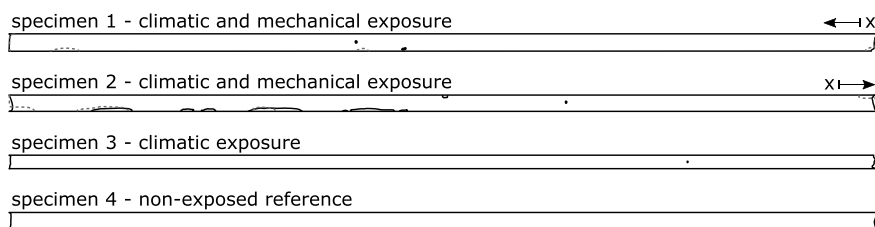


**Figure 14.** Cracks on the 400 mm-silicone beads of series B after exposure on the weathered side (solid line) and the opposite side (dashed line).

ascribed to different crack formation of specimen 1 and 2. In series B, small-scale specimens from specimen 2 have systematically lower strengths. The cracks decrease the bond area of the small-scale specimens and promote tearing of the silicone bond.

The dynamic moduli of the two system specimens in series B, shown in Figure 6, diverge during exposure. Hence, the more intense degradation of specimen 2 seems to be reflected in a stronger decrease of the dynamic moduli in x- and z-direction.

#### 4. Conclusion

The durability test method for SSG-systems proposed in this paper simultaneously applies climatic and mechanical loads to specifically designed medium-scale specimens. It provides a first comprehensive assessment of SSG-joint performance throughout an experimentally simulated service life of 50 years. From this exploratory research, that tested two common structural silicones in a custom-designed test facility, some conclusions can be drawn:

- Continuous mechanical characterisation yields dissipated energy and dynamic moduli in tension, compression and shear, which are useful parameters for characterisation of performance during exposure. The dissipated energy seems to be particularly sensitive towards ageing and fatigue of SSG-systems.
- Specimens of both test series bear at least 50 weathering cycles, with and without simultaneous mechanical loading. Performance characteristics consistently reflect differences between the two sealants, with higher moduli and dissipated energies in series A signalling increased mechanical resistance and damping capacity of sealant *a*.
- Discontinuous characterisations: tensile and shear tests of cut out small-scale specimens, hardness measurements, and visual inspection of the system specimens after exposure, supplement the continuous performance assessment. Strong crack formation, critical reduction in mean strength, and adhesive failure patterns in series B reveal limited durability

of sealant *b*, while sealant *a* passes the presented durability test. Future test procedures, though, should subject an increased number of specimens to tensile and shear tests for statistically significant durability assessment.

- A remarkable finding is that weather cycling alone has no significant effect on the characteristic mechanical parameters. Simultaneous climatic loading presumably contributes to the deterioration of the structural bond. To fully assess an interrelation of ageing and fatigue, future test series could additionally comprise mechanical loading at no simultaneous weathering.
- Practical implications of this study are technical improvements of the mechanical testing rig for a more homogeneous strain transfer into the sealant bead and the use of temperature-compensated strain sensors for more consistent effective loading at all ambient conditions.
- This study suggests improvements of currently regulated durability assessment of SSG-systems towards comprehensive performance-related durability testing at simultaneous mechanical and climatic loading.

## Funding

The first part of this work was supported by the German Federal Ministry of Economy and Technology under Grant MNPQ 22/10.

## ORCID

Wilma Wallau  <http://orcid.org/0000-0002-7111-0907>

## References

- [1] Klosowski, J.; Wolf, A. T. *Sealants in Construction*; CRC Press: Boca Raton, 2016; Vol. 2.
- [2] ASTM. C1401-14 Standard Guide for Structural Sealant Glazing. ASTM International. 2014. DOI: [10.1520/C1401-14](https://doi.org/10.1520/C1401-14).
- [3] Huang, Z.; Xie, M.; Chen, C.; Du, Y.; Zhao, J. Engineering Application of a Safety-state Evaluation Model for Hidden Frame-supported Glass Curtain Walls Based on Remote Vibration. *J. Build. Eng.* 2019, 26, 100915. DOI: [10.1016/j.jobbe.2019.100915](https://doi.org/10.1016/j.jobbe.2019.100915).
- [4] RWTH Aachen. Intelligent Structural Health Monitoring of Adhesive Joints in Facade Construction. 2020. <https://www.smartshm.rwth-aachen.de/intelligentes-shm-von-klebung-im-fassadenbau.html> (accessed May 29, 2020).
- [5] EOTA. ETAG 002 - Guideline for European Technical Approval for Structural Sealant Glazing Kit, Part 1: Supported and Unsupported Systems. May 2012.
- [6] Miyauchi, H.; Takemoto, Y.; Lacasse, M. A.; Tanaka, K. Development of an Automated Artificial Ageing Test Apparatus for Sealants and Comparison with Outdoor Exposure Testing. In 11th International Conference on the Durability of Building Materials and Components, Istanbul, Turkey, May 11-14, 2018. pp 1–10.

- [7] Wolf, A. T.; *Durability of Building Sealants: State-of-the-art Report of RILEM Technical Committee 139-DBS, Durability of Building Sealants*; RILEM publications SARL, 1999; Vol. 21.
- [8] Wolf, A. T.; RILEM TC190-SBJ: Development of Recommendations on Novel Durability Test Methods for Wet-applied Curtain-wall Sealants. *Mater. Struct.* **2008**, 41(9), 1473–1486. DOI: [10.1617/s11527-008-9418-2](https://doi.org/10.1617/s11527-008-9418-2).
- [9] Wolf, A. T.; Recommendation of RILEM TC 190-SBJ: Service-life Prediction of Sealed Building and Construction Joints. *Mater. Struct.* **2008**, 41(9), 1497–1508.
- [10] White, C. C.; Hunston, D. L.; Tan, K. T.; Filliben, J. J.; Pintar, A. L.; Schueneman, G. A Systematic Approach to the Study of Accelerated Weathering of Building Joint Sealants. *J. ASTM Int.* **2012**, 9(5), 1–17. DOI: [10.1520/JAI104091](https://doi.org/10.1520/JAI104091).
- [11] White, C. C.; Hunston, D. L.; Tan, K. T.; Hettenhouser, J.; Garver, J. D. An Accelerated Exposure and Testing Apparatus for Building Joint Sealants. *Rev. Sci. Instrum.* **2013**, 84(9), 095113. DOI: [10.1063/1.4821880](https://doi.org/10.1063/1.4821880).
- [12] Williams, R. S.; Lacher, S.; Halpin, C.; White, C. Evaluating Cyclic Fatigue of Sealants during Outdoor Testing. In *Service Life Prediction of Polymeric Materials*; Martin, J. W., Ryntz, R. A., Chin, J., Dickie, R. A., Eds.; Springer: Boston, **2009**; pp 129–151.
- [13] Williams, R. S.; Lacher, S.; Halpin, C.; White, C. Development of Test Apparatus for Service Life Prediction of Sealant Formulations and Evaluation of Data from 18 Months of Outdoor Weathering. In 4th International Woodcoatings Congress: Development for a Sustainable Future, Den Haag, Netherlands, October 25–27, **2004**.
- [14] Nardini, V.; Mueller, U. Optimized Adhesive for Structural Sealant Glazing in Blast Scenarios. *ce/papers*. **2018**, 2(5–6), 217–226. DOI: [10.1002/cepa.924](https://doi.org/10.1002/cepa.924).
- [15] Sugiyama, S.; Fatigue Resistance of Structural Glazing Silicone Sealants. In 3rd International RILEM Symposium on Durability of Building and Construction Sealants, Seneffe, Belgium, RILEM Publications SARL, **2000**. pp 97–111.
- [16] Sun, Y.; Wan, D.; Bao, Y.; Liu, X.; Qiu, Y. Study of Tensile Bond Strength for Structural Silicone Sealants after Artificial Accelerated Aging. *Key Eng. Mater.* **2018**, 768, 13–18.
- [17] You, X.; Wang, Z.-Y.; Shi, Y.; Luo, S. Dynamic Compressive Creep Behaviour of Structural Silicone-to-aluminum and Silicone-based Sealant- To-aluminum Joints. *J. Adhes. Sci. Technol.* **2019**, 33(21), 2293–2306. DOI: [10.1080/01694243.2019.1639587](https://doi.org/10.1080/01694243.2019.1639587).
- [18] Kaatz, R.; Recknagel, C.; Advanced Evaluation of Structural Sealant Glazing Systems by a New System Test Approach. *J. ASTM Int.* **2015**, STP 1583, 5, 376–402.
- [19] Wallau, W.; Recknagel, C. Test Methodology for Performance Assessment of Structural Sealant Glazing Systems at Superimposed Mechanical and Climatic Loading. *Polym. Test.* **2019**, 79, 106030. DOI: [10.1016/j.polymertesting.2019.106030](https://doi.org/10.1016/j.polymertesting.2019.106030).
- [20] Dow Corning Corporation. Silicone Structural Glazing Manual. Form Number: 62-0979H-01. **2011**.
- [21] Silvestru, V. A.; Englhardt, O.; Schneider, J. Investigations on Linear Silicone Joints for Glass-Metal Elements with Composite Structural Behavior. In Challenging Glass Conference Proceedings, Delft, Netherlands, May, **2018**. Vol. 6.
- [22] Meunier, L.; Chagnon, G.; Favier, D.; Orgéas, L.; Vacher, P. Mechanical Experimental Characterisation and Numerical Modelling of an Unfilled Silicone Rubber. *Polym. Test.* **2008**, 27(6), 765–777. DOI: [10.1016/j.polymertesting.2008.05.011](https://doi.org/10.1016/j.polymertesting.2008.05.011).
- [23] Hagl, A.; Development and Test Logics for Structural Silicone Bonding Design and Sizing. *Glass Struct. Eng.* **2016**, 1(1), 131–151. DOI: [10.1007/s40940-016-0014-5](https://doi.org/10.1007/s40940-016-0014-5).
- [24] Rey, T.; Chagnon, G.; Le Cam, J.-B.; Favier, D. Influence of the Temperature on the Mechanical Behaviour of Filled and Unfilled Silicone Rubbers. *Polym. Test.* **2013**, 32(3), 492–501. DOI: [10.1016/j.polymertesting.2013.01.008](https://doi.org/10.1016/j.polymertesting.2013.01.008).